Dalton Transactions

ROYAL SOCIETY OF CHEMISTRY

PAPER

View Article Online
View Journal | View Issue

Cite this: *Dalton Trans.*, 2025, **54**, 15271

808 nm near infrared excited Ho^{3+} and Tm^{3+} based metal–organic frameworks for luminescence thermometry and photothermal conversion

Albenc Nexha, *[a] Dasheng Lu,[b] Maria Cinta Pujol,[a] Jaume Massons,[a] Patricia Haro Gonzales, [c] Helene Serier-Brault [d] and Joan Josep Carvajal [a]

Received 28th June 2025,
Accepted 11th September 2025

DOI: 10.1039/d5dt01525a

rsc.li/dalton

Lanthanide based metal–organic frameworks are emerging as a class of materials with multiple applications. This is due to the combination of the unique optical properties of lanthanide ions and the extra functionalities added by the metal–organic frameworks. Nevertheless, up to now, these properties have not been explored to their full potential. In this work, we prove, for the first time, that Ho^{3+},Tm^{3+} based 1,3-benzenedicarboxylic acid metal–organic frameworks can be applied as luminescent thermometers and also as photothermal agents, using their upconversion properties after excitation at 808 nm.

Introduction

Metal–organic frameworks (MOFs) are hybrid materials, composed of metallic nodes and organic linkers.[1] MOFs are characterized by their high porosity levels, ranging from micro to meso-scale.[1] This property, combined with the high degree of variability for both inorganic and organic units within their structures, has boosted the application of MOFs in multiple fields.[1] Luminescence thermometry is a field that benefits from these unique properties of MOFs. It links the photoluminescence properties of a material with temperature to achieve thermal readouts.[2] This class of thermometry allows remote readouts and provides high spatial resolution in short acquisition times with high temperature resolution.[2] In addition, it operates under extreme conditions, such as under strong electromagnetic fields, at cryogenic temperatures and in biological fluids, without hampering the performance.[2,3] Due to its remote character, luminescence thermometry is becoming a pivotal tool for multiple areas, ranging from biomedicine, for example, in imaging, photothermal therapy and theranostics, to the Internet of Things as a data source platform.[2,3]

Among several phosphors applied as luminescent thermometers,[2] those based on lanthanide ions have advanced this field further. Due to their unique 4f–4f electronic configurations, these ions can modulate their radiative and non-radiative processes, responsible for the generation of photoluminescence and heat, respectively, when irradiated with a light source. When these processes are properly balanced, these materials can act as self-assessed photothermal agents.[4–6] Lanthanide ions exhibit stable and narrow photoluminescence covering a wide range of the electromagnetic spectrum, depending on the selected ion and optical transparency of the host.[2,7] The photoluminescence of the lanthanide ions could be triggered with ultraviolet (UV), visible (Vis) or near infrared (NIR) light.[2,7,8] In contrast to UV or Vis, excitation with NIR sources has found multiple advantages. For example, in biomedicine, these sources are harmless to biological matter and can penetrate deeper without producing autofluorescence.[2] Recently, in catalytic reactions, NIR sources have replaced the conventional UV or Vis light, which induces photocatalytic effects, altering the reaction itself.[9,10]

Lanthanide ions are usually doped into inorganic hosts,[2,7–9] which, although they have advanced the applicability of these ions in multiple fields, allow only low concentrations of the ions within their structures, due to the concentration quenching of their photoluminescence. This, in turn, leads to limited brightness and difficulties in distinguishing the signals of emissions from the background noise.[11] Although efforts are being made to design new structures to overcome this limitation, such as heavy doping a host with an emitting lanthanide ion,[12] they are still in progress.

In contrast, lanthanide based MOFs are not limited to the concentration of the ions. This is due to the 4f electrons of

[a]*Universitat Rovira i Virgili, Departament Química Física i Inorgànica, Campus Sescelades, E-43007 Tarragona, Spain. E-mail: albenc.nexha@leibniz-inm.de*
[b]*College of Rare Earths, Jiangxi University of Science and Technology, Ganzhou, 341000, PR China*
[c]*Nanomaterials for Bioimaging Group, Departamento de Física de Materiales, Instituto Nicolas Cabrera and Institute for Advanced Research in Chemical Sciences, Facultad de Ciencias, Universidad Autónoma de Madrid, Madrid 28049, Spain*
[d]*Université de Nantes, CNRS, Institut des Matériaux de Nantes Jean Rouxel, IMN, Nantes 44000, France*

lanthanide ions which enable high coordination numbers in the MOF structures, and due to the organic ligands which are excited in the absorption band and play the role of antennas to transfer energy to the emitting lanthanide ions.[13] State-of-the-art lanthanide based MOFs are mainly excited with UV or Vis irradiation.[13–17] For example, Tb^{3+} and Eu^{3+} ions are added into several types of MOFs due to their bright green and red emissions,[15–19] respectively. These emissions are triggered by using excitation wavelengths ranging from 289 nm to 395 nm.[15–19] In rare scenarios, MOFs based on Nd^{3+} and Yb^{3+} ions are excited with NIR laser sources, including 808 nm.[20,21] Nevertheless, their thermometric performance is based on the Stark sublevels of Nd^{3+} ions or the 980 nm emission of Yb^{3+} ions.[20,21] The Stark sublevels limit the performance up to the energy gap of the Nd^{3+} energy levels involved in sensing,[22] while the 980 nm emission of Yb^{3+} matches with the absorbance of water which limits significantly their application range.[23] Therefore, new strategies to develop more efficient thermometers based on NIR excitation sources are required. In addition, Nd^{3+} based MOFs should hold potential as photothermal agents; however, to date, this property has not been explored.[24]

Herein, we prepare Ho^{3+},Tm^{3+} based 1,3-benzenedicarboxylic acid MOFs, $[Gd_{1-x-y}Ho_xTm_y(CH_3COO)(1,3\text{-bdc})(H_2O)\cdot 0.5H_2O]$ (hereafter Ho,Tm:MOFs), *via* a solvothermal methodology.[15,16] The MOFs contain Ln_2 secondary building units as inorganic nodes in a 3D framework and ancillary ligands.[25,26] The selection of Ho^{3+} and Tm^{3+} is inspired by the ability of Tm^{3+} to absorb 808 nm excitation, generate emissions in the deep red region, and transfer this energy *via* energy transfer processes to Ho^{3+} ions, which emit in the green and red regions.[4–6] In addition, Tm^{3+} ions have multiple non-radiative channels, which are responsible for the generation of heat.[4–6] We analyse their ability to act as luminescent thermometers within the temperature range of 293 to 333 K. We also explore the possibility of using these materials as photothermal agents. Both these properties are triggered under irradiation with a NIR laser (808 nm). In contrast to the traditional 980 nm irradiation, which is absorbed by water and overheats the surrounding media,[23] 808 nm irradiation is barely absorbed by water.[7]

Experiments

Materials

$Tm(NO_3)_3\cdot 6H_2O$ (99.99%), $Ho(NO_3)_3\cdot 6H_2O$ (99.99%), $Gd(NO_3)_3\cdot 6H_2O$ (99.99%), 1,3-benzenedicarboxylic acid (99%) and NaOH (reagent grade 98%) were purchased from Alfa Aesar. Acetic acid (99.8%) was purchased from Acros Organics. All chemicals were used without further purification.

Synthesis of Ho,Tm:MOFs

Ho,Tm:MOFs were synthesized *via* a precipitation method performed at room temperature.[15,16] In brief, the ligand solution was prepared by dissolving 1,3-benzenedicarboxylic acid (115 mg, 0.69 mmol) in 5 mL of a NaOH solution (0.6 M) in deionized water. A cationic solution composed of lanthanide nitrate salts (0.69 mmol in total) was dissolved in 2 mL of deionized water containing glacial acetic acid (100 μL, 1.7 mmol). The cationic solution was added dropwise to the ligand solution. The pH of the mixture was adjusted to 5.0 by adding a NaOH solution (1.5 M, in deionized water). The white mixture was stirred for 30 minutes at room temperature. The as-obtained white powder was finally recovered by filtration and washed with EtOH. Two chemical compositions were synthesized, $Gd_{0.92}Ho_{0.03}Tm_{0.05}$ (named 3Ho,5Tm hereafter) and $Gd_{0.89}Ho_{0.01}Tm_{0.10}$ (named 1Ho,10Tm hereafter), with yields around 40%.

Luminescence thermometry of Ho,Tm:MOFs

The photoluminescence of the Ho,Tm:MOFs was recorded in the range of 500 nm to 800 nm using a CCD camera. The samples were excited using a near infrared 808 nm fiber coupled diode laser at different powers (ranging from 5 to 20 mW). The scattered excitation radiation was eliminated by using an 850 nm long-pass dichroic filter. For temperature dependent photoluminescence measurements, the same optical setup was used, except that the sample was located on a heating plate. The performance of these samples as luminescent thermometers was analysed within the temperature range of 293 K to 333 K.

Photothermal conversion efficiency of Ho,Tm:MOFs

The prepared samples as powders were deposited on a well plate, made of cellulose bioplastic, uniformly covering a circular area of 4 mm in diameter and 0.5 mm in height. The particles were excited at 808 nm with a power of 25 mW. The laser was coupled with a multimode fibre with a core diameter of 400 μm, connected to a collimator (FOC-01 from CNI Laser). The position of the laser beam was fixed using a monochromic camera (DMK 23U445 from The Imaging Source). The temperature profiles of the samples were recorded using an infrared camera (VarioCam@HD 980 S from InfraTec), positioned 10 cm above the samples. The thermal resolution of the infrared camera is 0.02 K. The irradiated area was continuously irradiated for 10 min and a temperature map was recorded every 30 s to follow the heating process and extract the temperature profiles.

Characterization of Ho,Tm:MOFs

The crystalline structure of the Ho,Tm:MOFs was investigated *via* X-ray powder diffraction (XRD) using a D8 Bruker diffractometer in the Bragg–Brentano geometry, equipped with a front germanium monochromator, a copper anode ($Cu_{K\text{-}L3}$ radiation λ = 1.54 Å) and a LynxEye PSD detector. The Raman active vibrational modes of the materials were recorded *via* micro-Raman analysis, using a Renishaw inVia Reflex microscope with unpolarized 532 nm light focused on the sample with a 50× Leica objective in the range of 200–2000 cm^{-1}, using a grating with 1200 lines per mm and an exposure time of 10 s. Thermogravimetric analyses (TGA) were performed by flowing

dry air with a heating rate of 5 K min^{-1} on a SETARAM TG-DSC 111 machine operating between room temperature and 1073 K. Scanning electron microscopy (SEM) and energy-dispersive X-ray spectroscopy (EDX) were conducted on a Zeiss Gemini 500 microscope equipped with an EDX detector from Oxford Instruments. An acceleration voltage between 1 kV and 15 kV was used to acquire the data. Fourier transform infrared (FT-IR) spectra were recorded in the 4000–400 cm^{-1} range on a Bruker Vertex FTIR spectrometer equipped with a computer control using the OPUS software. For ICP-AES analyses, the samples were dissolved in a 10% HNO_3 solution and analyzed by ICP-AES. The calibration curve was established from the analysis of five standard solutions containing Gd^{3+}, Ho^{3+}, and Tm^{3+} at various concentrations.

Results and discussion

Characterization of Ho,Tm:MOFs

Using a precipitation method performed at room temperature,[15,16] two MOF materials doped with Ho^{3+} and Tm^{3+} (3 mol% Ho^{3+} and 5 mol% Tm^{3+} as 3Ho,5Tm, and 1 mol% Ho^{3+} and 10 mol% Tm^{3+} as 1Ho,10Tm, respectively) were prepared. White microcrystalline powders were obtained as the final products with yields around 40%.[15,16] First, structural characterization of the products was conducted. Powder X-ray diffraction (XRD) patterns (Fig. 1(A)) reveal that the synthesized MOFs are isostructural with the $Ln(CH_3COO)(1,3\text{-bdc})(H_2O)_2{\cdot}0.5H_2O$ compounds (Ln = Gd, Sm, Nd, Sm, Eu, La).[25,26] Each Ln^{3+} is nine-coordinated in tricapped trigonal prismatic geometry (formed by nine O-atoms from three different 1,3-bdc^{2-} ligands, two distinct acetate ligands, and two water molecules) (Fig. S1 in the SI). Unpolarized Raman spectroscopy confirms multiple strong bands at 1000 cm^{-1} and 1400–1600 cm^{-1}, assigned to the vibrational groups (C═O, O–H, C═C) (section I: Fig. S2(a) in the SI). FT-IR data reveal that the surface of the prepared structures is dominated by organic moieties (section I: Fig. S2(b) in the SI). Thermogravimetric analyses (TGA) show identical profiles and mass losses up to 1000 K (Fig. 1(B)), with an initial 10% loss due to the removal of water molecules, followed by nearly 50% loss assigned to the total decomposition of the material. The morphology of the synthesized materials was characterized using SEM. The particles are composed of aggregated flake-like structures (Fig. 1(C)). An energy-dispersive X-ray spectroscopy (EDX) spectrum was acquired to identify the composition of the synthesized products. EDX confirms the presence of all metals involved in the synthesis (Fig. 1(D)). The elemental mapping reveals the uniform distribution of Gd, Ho, and Tm, as well as the organic moieties from C and O (Fig. S3 in the SI). The molar ratios of Gd, Ho and Tm in the compounds were determined by ICP-AES (Table S1 in the SI), and the derived nominal compositions are $Gd_{0.90}Ho_{0.04}Tm_{0.06}$ (3Ho,5Tm) and $Gd_{0.88}Ho_{0.008}Tm_{0.112}$ (1Ho,10Tm). All these techniques confirm that the substitution of Gd^{3+} by Tm^{3+} and Ho^{3+} in the MOFs did not affect their structure.

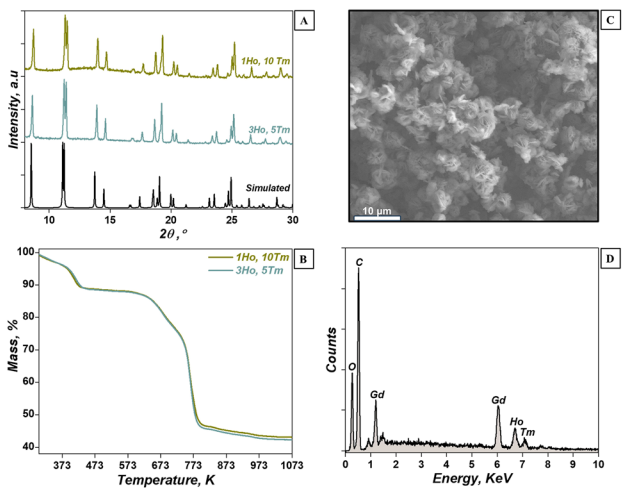

Fig. 1 Characterization of the synthesized Ho,Tm:MOF materials: (A) XRD patterns, (B) TGA data, (C) SEM micrograph, and (D) EDX spectrum.

Photoluminescence of Ho,Tm:MOFs

Next, we tested whether the upconversion photoluminescence of the lanthanide ions could be generated within the synthesized MOFs. For that, the Ho,Tm:MOFs were excited with near infrared light (λ_{exc} = 808 nm). This excitation wavelength is not absorbed by water in the environment surrounding the MOFs.[2] Two different compositional ratios were selected: 3 mol% Ho^{3+} and 5 mol% Tm^{3+} (sample 3Ho,5Tm) and 1 mol% Ho^{3+} and 10 mol% Tm^{3+} (sample 1Ho,10Tm). These two ratios were previously optimized to generate bright emissions of these lanthanide ions when embedded into other hosts.[4–6] After excitation at 808 nm, the upconversion photoluminescence of these samples, in solid state, was recorded within the visible range at room temperature. The spectra consist of emission bands located in the green, red and deep red regions (Fig. 2(A)). The bands at 550 nm and 650 nm are assigned to the Ho^{3+} ion. On the other hand, the Tm^{3+} ion emits at around 700 nm.[5] Here, Tm^{3+} acts as a sensitizer, *i.e.* it absorbs the 808 nm irradiation and uses this energy, partially, to generate the emissions at around 700 nm, while part of it is transferred to Ho^{3+} to generate the emissions in the red and green regions. Shortly afterwards, Tm^{3+} ions absorb the energy of the excitation source to populate their $^1G_4$ excited state, from which a non-radiative process populates the $^3F_{2,3}$ state. From this state, a radiative decay to the ground level $^3H_6$ generates the deep red emission of this ion (Fig. 2(B)). The green and red emissions of Ho^{3+} ions are generated due to an energy transfer (ET) process from Tm^{3+}. From the $^3F_4$ level of Tm^{3+}, an ET process can populate the $^5I_7$ level of Ho^{3+} (Fig. 2(B)). From this level, an additional ET can promote the electrons of Ho^{3+} to higher energy levels ($^3K_8$ and $^5F_3$). After a non-radiative process that populates the $^5S_2$ and $^5F_4$ levels, a direct radiative process to the ground state $^5I_8$ generates the green emission of Ho^{3+} at 550 nm. Another non-radiative process from the $^5F_4$ and $^5S_2$ levels populates the $^5F_5$ level, which upon relaxing

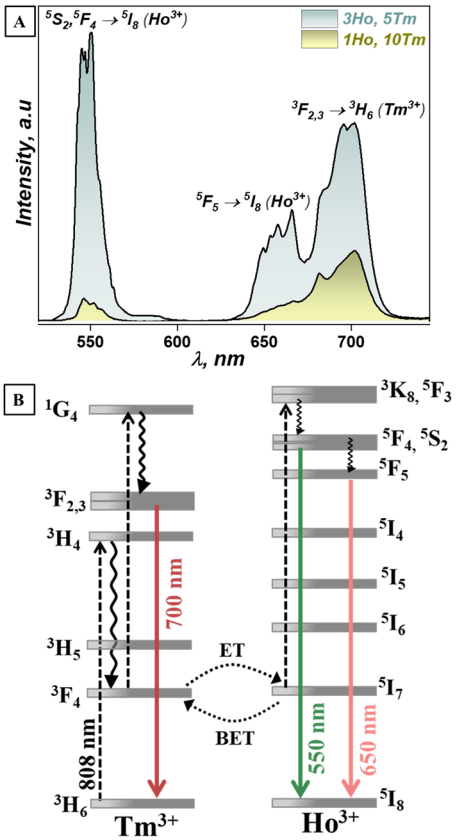

Fig. 2 (A) Photoluminescence and (B) upconversion mechanism for the generation of visible light in the Ho,Tm:MOFs under NIR 808 nm excitation.

radiatively to the ground state, generates the red emission around 655 nm (Fig. 2(B)).

In terms of photoluminescence intensity, the 3Ho,5Tm sample exhibits more intense upconversion emissions compared to those generated by the 1Ho,10Tm sample. This is due to a more effective ET process taking place for the 3Ho,5Tm sample, containing a higher amount of Ho^{3+}, as previously described.[4] On the other hand, although the 1Ho,10Tm sample exhibits a lower emission intensity in general compared to the 3Ho,5Tm sample, the deep red emission of Tm^{3+} is dominant compared to the bands of Ho^{3+}. This is due to the increase in the concentration of Tm^{3+} up to 10 mol%. Given the significantly higher emission intensity obtained on the 3Ho,5Tm sample, it was further characterized as a luminescent thermometer.

Ho,Tm:MOFs as luminescent thermometers

After confirming the photoluminescence of the lanthanide ions, we explored the possibility of using these materials as luminescent thermometers. For this, the photoluminescence of the 3Ho,5Tm sample was recorded as a function of temperature from 293 to 333 K. The thermometric performance was evaluated by calculating the relative thermal sensitivity and the temperature resolution, two parameters used as figures of merit for thermometers, regardless of their nature, operating wavelengths, or experimental parameters used to acquire their thermometric parameter.[2]

With the increase of temperature, the intensity of all the emission bands was quenched. The green (550 nm as I_1) and red (650 nm as I_2) emission bands of Ho^{3+} ions decreased up to 70% and 62% of their initial values, respectively (Fig. 3(A) and (B)). On the other hand, the intensity of the deep red (700 nm as I_3) emission band of Tm^{3+} ions was reduced up to 29% of its initial value (Fig. 3(A) and (B)). We used the intensity ratios among these three emission bands to extract the thermometric performance. Thus, all intensity ratios decrease with the increase of temperature (Fig. 3(C)). The experimental data were fitted to a phenomenological exponential equation since the electronic levels from which these emissions arise are not thermally coupled.[5] We used the following equation to fit the experimental data of the intensity ratios (Δ):[5]

$$\Delta = \Delta_0 + B\exp(\alpha T) \quad (1)$$

where Δ_0 and B are constants to be determined by the fitting. All experimental data match with the proposed equation with excellent R^2 values in the range of 0.98 to 0.99 (Fig. 3(C) and Table S2 in the SI). Δ_1, Δ_2 and Δ_3 are the intensity ratios among I_1 *vs.* I_2, I_1 *vs.* I_3, and I_2 *vs.* I_3, respectively. From this equation, we can calculate the values of the relative thermal sensitivity (S_{rel}) and the temperature resolution (δT). S_{rel}, which stands for the relative change in the thermometric parameter (Δ) for each temperature degree, is defined as:[2,5]

$$S_{rel} = \frac{1}{\Delta}\left|\frac{\partial\Delta}{\partial T}\right| \times 100\%. \quad (2)$$

After substituting eqn (1) in eqn (2), the expression for the determination of S_{rel} is:

$$S_{rel} = \frac{B\alpha\exp(\alpha T)}{\Delta_0 + B\exp(\alpha T)} \times 100\%. \quad (3)$$

Among the three intensity ratios under investigation, the intensity ratio between the Ho^{3+} band at 550 nm and the Tm^{3+} band at 700 nm (Δ_2) showed the highest S_{rel} with a value of 7.3% K^{-1} at 333 K (Fig. 3(D)). The intensity ratio between the two Ho^{3+} emission bands (Δ_1) exhibited the lowest S_{rel} with a value of 3.31% K^{-1} at the same temperature (Fig. 3(D)).

On the other hand, δT, which expresses the minimum temperature change that a thermometer can resolve, is defined as:[2,5]

$$\delta T = \frac{1}{S_{rel}}\frac{\delta\Delta}{\Delta} \quad (4)$$

where $\frac{\delta\Delta}{\Delta}$ is the relative error in the determination of the thermometric parameter from the detection setup, and in this work, we considered a standard value of 0.5%.[5] A smaller δT implies a better thermometric performance.[2] Among the three intensity ratios analysed, the ratio between the Ho^{3+} emission band at 550 nm and the Tm^{3+} emission band located at 700 nm exhibited the smallest δT with a value of 0.068 K at

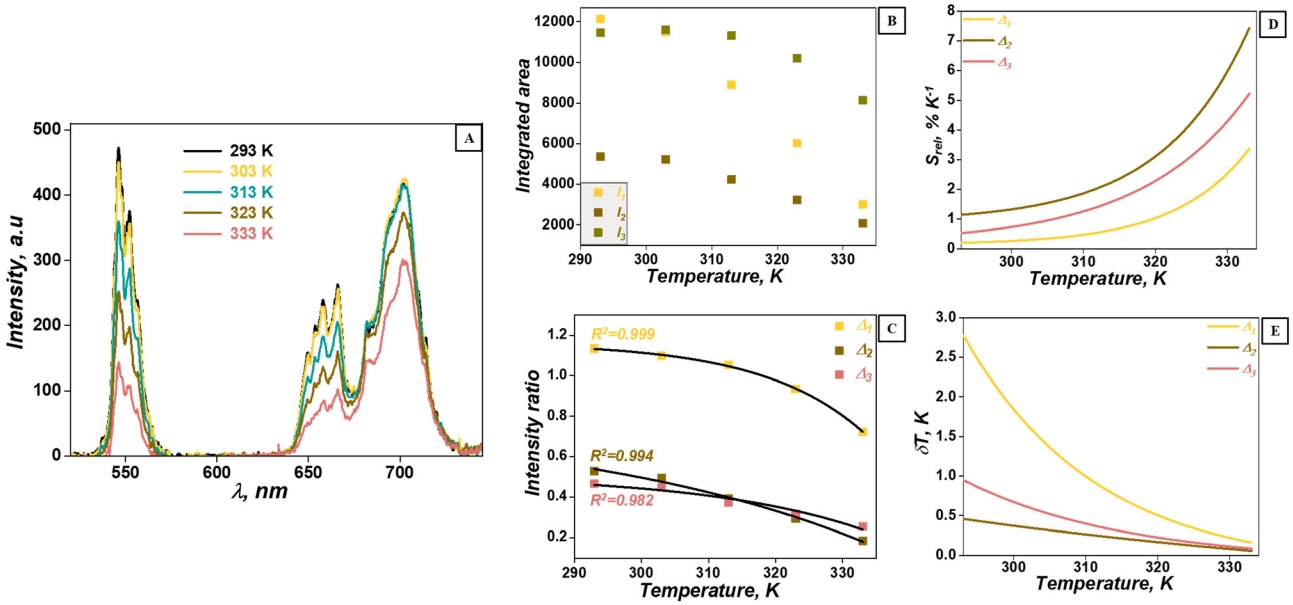

Fig. 3 Temperature dependence (293 K to 333 K) of (A) photoluminescence spectra, (B) intensities, (C) intensity ratios, (D) relative thermal sensitivities, and (E) temperature resolutions among the three emission bands of the 3Ho,5Tm sample. Intensities I_1, I_2 and I_3 are assigned to the bands located at 550 nm (Ho^{3+}), 650 nm (Ho^{3+}), and 700 nm (Tm^{3+}), respectively. The particles are excited with an 808 nm laser operating at a power of 10.5 mW.

333 K (Fig. 3(E)), although the value is below 0.5 K in the whole range of temperatures analysed.

After determining the thermometric performance of the Ho,Tm:MOFs, we can compare them with other state-of-the-art thermometers using the reported S_{rel} values.[2,7] First, we compare the performance among other hosts containing Ho^{3+} and Tm^{3+}, either single doped or codoped. When codoped into double tungstate $KLu(WO_4)_2$, the maximum S_{rel} achieved was around 1.9% K^{-1} at room temperature.[5] Similarly, when single doped, for example Tm^{3+} into LaF_3,[27] or Ho^{3+} into $Na(Y,Gd)F_4$[28] (Gd included to enhance the green and red emissions of Ho^{3+} ions), their maximum S_{rel} reached values of 2.9% K^{-1} and 1.2% K^{-1} at room temperature, respectively (Fig. 4). Clearly, the Ho,Tm:MOFs achieve 5 to 6-fold higher S_{rel} compared to these ions when embedded into inorganic hosts, and more importantly, the maximum S_{rel} values were achieved at temperatures above room temperature, which make these thermometers more interesting for applications in which better temperature resolutions are needed at these temperatures.

We can also compare the thermometric performances of the Ho,Tm:MOFs with other luminescence based MOF thermometers. In the state of the art, other lanthanide ions have been added into MOFs and their thermometric properties have been investigated. For example, Nd^{3+} and Yb^{3+} ions were added into $Ln(BTB)(H_2O)$ MOFs (where BTB = 1,3,5-benzenetrisbenzoic acid).[21] Their thermometric performance, extracted within the physiological range of temperatures, was deduced from the intensity ratio among the emissions of Nd^{3+} at 1060 nm and Yb^{3+} at 980 nm.[21] Their maximum S_{rel} was reached at 333 K with a value of 4.75% K^{-1}.[21] The most

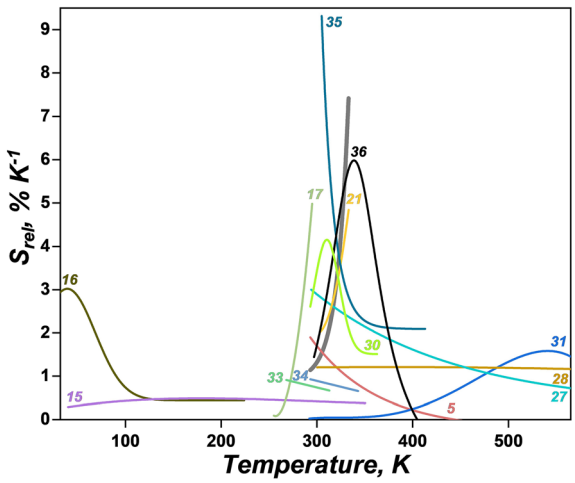

Fig. 4 Temperature dependence of the relative thermal sensitivity of different types of thermometers (numbers stand for references from which the data were extracted). Ho,Tm:MOF thermometers are presented in a gray line.

popular combination of lanthanide ions for thermometry using MOFs is Eu^{3+} and Tb^{3+}, although they are mainly sensitive at low temperatures.[14,29] For example, Eu^{3+} and Tb^{3+} were added into isophthalic acid based MOFs, the same building blocks as for the Ho,Tm:MOFs explored here. Their ability to sense temperature was investigated in the cryogenic range of temperatures,[16] and also at room temperature,[15] taking into account the green and red emissions of Tb^{3+} and Eu^{3+}, respectively. Their S_{rel} within the cryogenic range of temperatures was

around 7-fold higher than the one achieved at room temperature (Fig. 4). The maximum value was 3.26% K^{-1} at 35.5 K.[16] Other Eu^{3+},Tb^{3+} based MOFs sensitive around and beyond room temperature have been recently reported. Thus, Eu^{3+}, Tb^{3+} based UiO-66 when grafted into a covalent organic framework (COF) achieved a maximum S_{rel} value of 4.9% K^{-1} at 295 K,[17] and 4.1% K^{-1} at 315 K.[30] When Eu^{3+} and Tb^{3+} were added into a yttrium based MOF, S_{rel} was around 1.69% K^{-1} at 523 K.[31] However, all these sensitive thermometers must be excited under UV irradiation, which limits the applications of these materials given the phototoxicity effect generated from this light source.[32]

Finally, we compare our thermometers with others based on inorganic hosts doped with emitting lanthanide ions. The well-known green emitting Er^{3+} ions when doped into single hexagonal $NaYF_4$, or prepared as core@shell structures and embedded into UiO-66-NH_2, exhibit a limited S_{rel} around 1% K^{-1},[33,34] which is nearly 8-fold lower (Fig. 4). A recent trend to improve the performance of thermometers relies on designing particles with opposite thermal responses (thermal quenching and thermal enhancement). A core@shell@shell nanorod structure (Nd^{3+},Yb^{3+}:$NaYF_4$@$NaYF_4$@Er^{3+},Yb^{3+}:$NaYF_4$) was designed to combine the thermally enhanced emission of Nd^{3+} (at 803 nm) and the thermally quenched emission of Er^{3+} (at 654 nm) for thermometry.[35] The maximum S_{rel} was as high as 9.6% K^{-1} at room temperature (Fig. 4). Although this value is higher than that of the Ho,Tm:MOF thermometers, the protocols for producing these types of particles are time-consuming and in addition, their emissions are triggered with a 980 nm laser. Other strategies for achieving higher S_{rel} include merging small (17 nm) and big (70 nm) upconverting nanoparticles.[36] The small particles were doped with Tm^{3+} ions, whose blue emission was thermally enhanced with the increase of temperature. The big particles, doped with Er^{3+} ions, exhibited gradual quenching of the green emission. Using this ratio, S_{rel} was around 5.88% K^{-1} at 339 K (Fig. 4). Yet again, these particles were excited with a 980 nm laser.

Consequently, Ho,Tm:MOF materials offer a promising alternative to mixed Eu^{3+},Tb^{3+}:MOFs, regardless of their very high thermometric performances around room temperature. Furthermore, compared to the inorganic host, their potential porosity could bring additional properties, such as active molecule delivery.[13] In addition, these optical properties are triggered by a wavelength not absorbed by water molecules, such as 808 nm, a key advantage for multiple applications.

The high S_{rel} of the Ho,Tm:MOF thermometers could be linked to the presence of water molecules on their structure [$(Ln(CH_3COO)(1,3\text{-bdc})(H_2O)_2{\cdot}0.5H_2O)$, where Ln = Gd, Ho, Tm]. According to the TGA data (Fig. 1(B)), the material loses up to 5% of their mass at around 333 K, assigned to the removal of water molecules from the structure. Therefore, these structures could exhibit similar properties to thermoresponsive polymers,[37] with the OH^- groups acting as quenchers for the luminescence of the lanthanide ions.[38] However, compared to the polymers whose structures are destroyed, the structure of the MOFs should remain intact within the temperature range explored for thermometry. To confirm this, we examined the structure and the surface of the samples *via* XRD and Raman spectroscopy, respectively. The crystalline structure of the material is preserved as confirmed by the comparison of the XRD patterns before and after exposure to 333 K (Fig. 5(A)). In addition, from the Raman spectra recorded before and after exposure to 333 K, there are no clear changes in the vibrational modes of the materials (Fig. 5(B)). These analyses confirm the stability of the structure of the materials after exhibiting their thermometric properties.

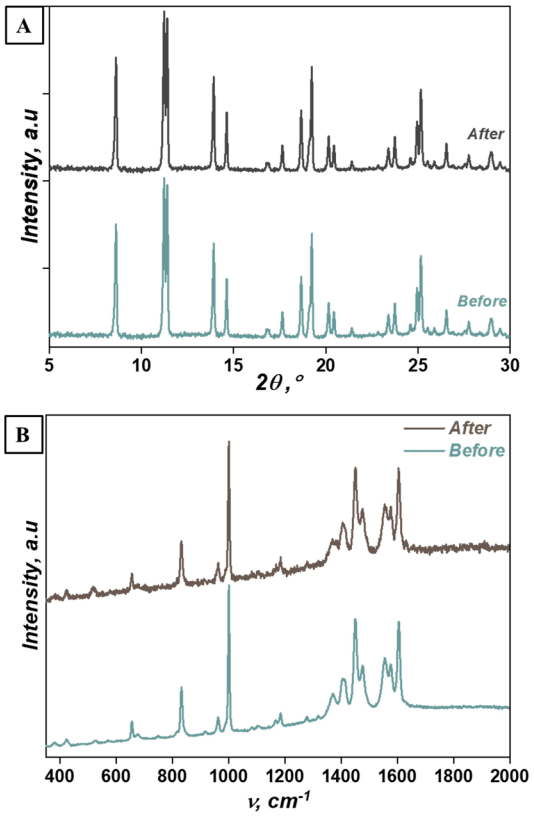

Fig. 5 (A) XRD patterns and (B) Raman spectra of 3Ho,5Tm before (in blue) and after (in black) exposure at 333 K for 5 hours.

Ho,Tm:MOFs as photothermal agents

We also investigated the possibility of the Ho,Tm:MOFs generating heat when irradiated with an 808 nm laser, as previously demonstrated in inorganic hosts.[4–6] Heat is generated due to the non-radiative processes happening in Tm^{3+} ions (Fig. 2(B)). This heat generation can be used for different purposes, such as promoting catalytic reactions or thermal treatment of materials. Considering the luminescent thermometric possibilities of these materials, this would allow for assessing simultaneously the temperature of the medium surrounding the luminescent material heated by this same material.[4,6] To prove this property in the synthesized MOFs, they were continuously irradiated with an 808 nm laser with a power of 25 mW for 10 min. A thermal camera was used to visualise the heating process and extract the temperature profiles.

Both samples exhibit a similar behaviour under 808 nm irradiation: a significant increase in temperature is observed within the first few minutes, followed by asymptotic stabilization (Fig. 6, Movies S1 and S2 for 3Ho,5Tm and 1Ho,10Tm in the SI, respectively). Within the first three minutes, the maximum temperature was achieved (Movies S1 and S2 in the SI). The 3Ho,5Tm sample achieved a maximum temperature of 304.6 K, while for the 1Ho,10Tm sample, the maximum temperature reached was 311.1 K (Fig. 6(A) and (B)). Within the next seven to eight minutes, these temperatures remained stable without major changes. The results are also confirmed from temperature profiles recorded along the lateral diameter of the well, as a function of time (Fig. 6(C) and (D)). The 1Ho,10Tm sample generated more heat compared to the 3Ho,5Tm sample. This is in agreement with what has been observed in inorganic hosts doped with these ions, where a higher concentration of Tm^{3+} ions leads to a higher probability of non-radiative processes taking place, and consequently, a higher amount of energy dissipating in the form of heat.[4,5]

We calculated the photothermal conversion efficiency of these materials. For that, the maximum temperature data as a function of time (Fig. 6(C) and (D)) were fitted to an asymptotic exponential function obtained from the Fourier law. The temperature $T(t)$ obtained from this model is given by:[39]

$$T(t) - T_{amb} = (T_{max} - T_{amb})\left(1 - e^{\left(-\frac{t}{\tau}\right)}\right) \quad (5)$$

where T_{amb} is the ambient temperature (*i.e.* the temperature at $t = 0$), T_{max} is the temperature in the steady-state regime and τ is the time constant associated with the thermal circuit. τ could be expressed as the product of the thermal resistance of the system R and the heat capacity C:

$$\tau = R \times C \quad (6)$$

The heat capacity is extracted from the product of the mass of the heat material m and the specific heat c_p:

$$C = m \times c_p \quad (7)$$

On the other hand, the maximum temperature T_{max} in the steady state can be calculated from:[39]

$$(T_{max} - T_{amb}) = P_{abs} \times R \quad (8)$$

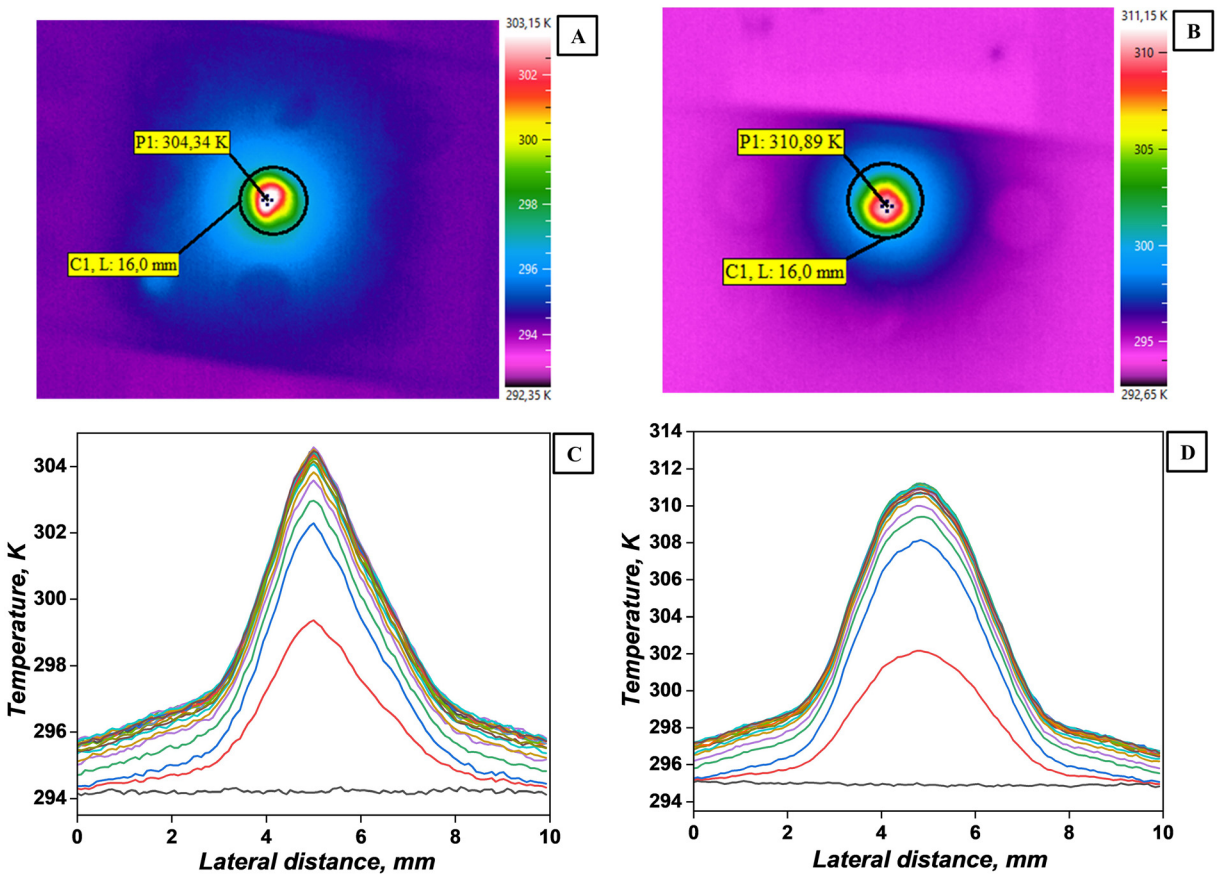

Fig. 6 Steady state thermal maps and temperature profiles along the diameter of the irradiated area for the (A and C) 3Ho,5Tm and (B and D) 1Ho,10Tm samples under 808 nm laser continuous irradiation for 10 minutes with a power of 25 mW. Temperature profiles are delayed by 30 s from each other.

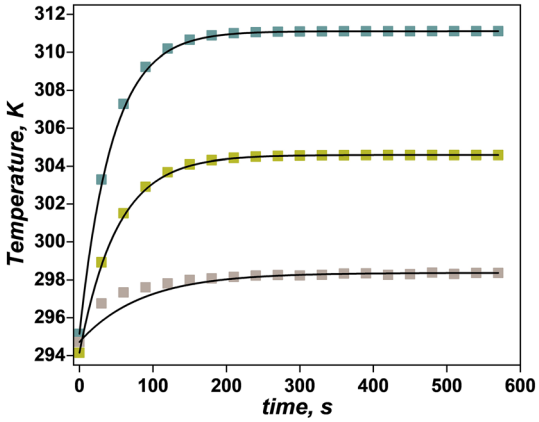

Fig. 7 Time evolution of the temperature at the center of the irradiated area for the 3Ho,5Tm (blue) and 1Ho,10Tm (green) and Gd^{3+} based MOF (in brown) samples: symbols and solid lines stand for experimental data and fitted data to eqn (5), respectively.

where P_{abs} stands for the heat power absorbed by the heated element. Eqn (8) is used to determine the thermal resistance of the system.

Fitting the experimental data to eqn (5) generates a T_{max} of 304.6 K and a τ of 49 s for the 3Ho,5Tm sample (Fig. 7). The data of the 1Ho,10Tm sample generate a T_{max} of 311.1 K and a τ of 42 s. T_{amb} was 294 K and 295 K for the 3Ho,5Tm and 1Ho,10Tm samples, respectively. P_{abs} was determined from a parametric heat transfer model (section II in the SI). The P_{abs} values were 8.5 mW and 14 mW for 3Ho,5Tm and 1Ho,10Tm, respectively. After determining the values of P_{abs}, the heating efficiency (η) could be calculated, reaching 34% and 56% for 3Ho,5Tm and 1Ho,10Tm, respectively. As expected, η increases as the concentration of Tm^{3+} ions increases.[4] In addition, to elucidate that the heating is assigned only to the non-radiative processes in the Ho,Tm doped samples, we prepared a reference sample composed of only Gd^{3+}. After being irradiated with the laser, this sample exhibited a maximum increase of temperature of only 4 K, substantially lower than that of the Ho,Tm based samples (Fig. 7).

The thermal resistance R of both configurations is 1.22×10^3 K W^{-1} and 1.19×10^3 K W^{-1} for 3Ho,5Tm and 1Ho,10Tm, respectively. These values are similar as the effective heated volume mainly involves the material of the sample holder. The heat capacities are calculated as 33.2×10^{-3} and 38.6×10^{-3} J K^{-1} for 3Ho,5Tm and 1Ho,10Tm, respectively. Considering that the c_p of cellulose, composing the holder, is around 1200 J kg^{-1} K^{-1},[40] the effective heated masses, obtained from eqn (7), are 33.2 mg and 32.2 mg for 3Ho,5Tm and 1Ho,10Tm, respectively. Note that these masses are much higher than the amount of MOF deposited on the sample holder, justifying the above hypothesis that the heated material is mainly the cellulose of the holder.

Conclusions

In summary, we explored for the first time the radiative and non-radiative processes of Ho^{3+} and Tm^{3+} in a MOF matrix by irradiation with a NIR 808 nm laser source. Due to their radiative process, these materials can act as highly sensitive luminescent thermometers. They substantially improve the performance of state-of-the-art luminescent thermometers, regardless of the host, operating temperatures, or spectral regions, reaching values of S_{rel} up to 6-fold higher. The maximum value of S_{rel} was 7.3% K^{-1} recorded at 333 K. Due to the benefit provided by the non-radiative processes in these ions, we also investigated the possibility of heat generation, which renders them as candidates for self-assessed photothermal agents for multiple applications. These materials exhibit a high photothermal conversion efficiency with a value of around 56%. In addition, the MOFs used as hosts are not only stable in these experiments but also might provide extra functionalities, such as reservoirs for chemicals.[41] In this way, in the near future, we can aim to develop a multifunctional nanosized structure that benefits from the properties of the two building blocks, which can tackle challenges in biomedicine. This structure holds the potential to impact other fields, such as photocatalysis,[10] for example acting as a light generator or triggering heat to start catalysis. The structure will provide insights into the temperature changes during photocatalysis, allowing a closer control over the chemical reactions. Another potential application might be solar energy harvesting. From one side, the solar photo flux at 808 nm is higher than that at 980 nm, reducing the impact from water molecules. On the other side, NIR light is converted into Vis light in the region of maximum absorption of silicon, resulting in more efficient harvesting.[10] In this case, heat generation processes and their monitoring by the same material can be applied to control the temperature of the device, and set up the temperatures to make it work under the optimal conditions, also preventing its failure due to excess temperature.

Author contributions

Helene Serier-Brault synthesized the lanthanide doped metal–organic frameworks. Dasheng Lu and Albenc Nexha performed the experiments on luminescence thermometry and photothermal conversion efficiency. Jaume Massons simulated the photothermal conversion efficiency. Joan Josep Carvajal, Maria Cinta Pujol, and Patricia Haro Gonzales led the supervision and funding acquisition. All authors took part in the conceptualization, reviewing, and editing of the manuscript.

Conflicts of interest

There are no conflicts to declare.

Data availability

The data that support the findings of this study are available from the corresponding author upon request.

Supplementary information is available. See DOI: **https://doi.org/10.1039/d5dt01525a**.

Acknowledgements

This work was supported by grant PID2021-128090OB-C22 funded by MICIU/AEI/10.13039/501100011033 and ERDF/UE and by grant 2021 SGR 00658 funded by Generalitat de Catalunya.

References

1 H. C. Zhou, J. R. Long and O. M. Yaghi, Introduction to metal-organic frameworks, *Chem. Rev.*, 2012, **112**, 673–674.
2 A. Nexha, J. J. Carvajal, M. C. Pujol, F. Díaz and M. Aguiló, Lanthanide doped luminescence nanothermometers in the biological windows: strategies and applications, *Nanoscale*, 2021, **13**, 7913–7987.
3 J. J. C. Martí and M. C. P. Baiges, *Luminescent Thermometry: Applications and Uses*, Springer Nature, 2023.
4 A. Nexha, J. J. Carvajal, M. C. Pujol, F. Díaz and M. Aguiló, Short-wavelength infrared self-assessed photothermal agents based on Ho,Tm:KLu$(WO_4)_2$ nanocrystals operating in the third biological window (1.45–1.96 μm wavelength range), *J. Mater. Chem. C*, 2020, **8**, 180–191.
5 A. Nexha, J. J. Carvajal, M. C. Pujol, F. Díaz and M. Aguiló, Synthesis of monoclinic Ho,Tm:KLu$(WO_4)_2$ microrods with high photothermal conversion efficiency via a thermal decomposition-assisted method, *J. Mater. Chem. C*, 2021, **9**, 2024–2036.
6 A. Nexha, M. C. Pujol, J. J. Carvajal, F. Díaz and M. Aguiló, Effect of the size and shape of Ho,Tm:KLu$(WO_4)_2$ nanoparticles on their self-assessed photothermal properties, *Nanomaterials*, 2021, **11**, 485.
7 A. Nexha, M. C. Pujol and J. J. Carvajal, in *Luminescent Thermometry: Applications and Uses*, ed. J. J. Carvajal and M. C. Pujol, Springer International Publishing, Cham, 2023, pp. 221–268, DOI: 10.1007/978-3-031-28516-5_6.
8 A. Nexha, S. Mariani, K. Cikalleshi, T. Kister, B. Mazzolai and T. Kraus, Sensing relative humidity with a fluorescent seed-like biodegradable flier, *Nanoscale*, 2025, **17**, 18143–18152.
9 C. D. S. Brites, S. Balabhadra and L. D. Carlos, Lanthanide-based thermometers: At the cutting-edge of luminescence thermometry, *Adv. Opt. Mater.*, 2019, **7**, 1801239.
10 B. S. Richards, D. Hudry, D. Busko, A. Turshatov and I. A. Howard, Photon upconversion for photovoltaics and photocatalysis: A critical review, *Chem. Rev.*, 2021, **121**, 9165–9195.
11 Z. Wang and A. Meijerink, Concentration quenching in upconversion nanocrystals, *J. Phys. Chem. C*, 2018, **122**, 26298–26306.
12 S. Wen, J. Zhou, K. Zheng, A. Bednarkiewicz, X. Liu and D. Jin, Advances in highly doped upconversion nanoparticles, *Nat. Commun.*, 2018, **9**, 2415.
13 F. Saraci, V. Quezada-Novoa, P. R. Donnarumma and A. J. Howarth, Rare-earth metal-organic frameworks: from structure to applications, *Chem. Soc. Rev.*, 2020, **49**, 7949–7977.
14 J. Rocha, C. D. S. Brites and L. D. Carlos, Lanthanide Organic Framework Luminescent Thermometers, *Chem. – Eur. J.*, 2016, **22**, 14782–14795.
15 V. Trannoy, A. N. Carneiro Neto, C. D. S. Brites, L. D. Carlos and H. Serier-Brault, Engineering of mixed Eu^{3+}/Tb^{3+} metal-organic frameworks luminescent thermometers with tunable sensitivity, *Adv. Opt. Mater.*, 2021, **9**, 2001938.
16 I. N'Dala-Louika, D. Ananias, C. Latouche, R. Dessapt, L. D. Carlos and H. Serier-Brault, Ratiometric mixed Eu-Tb metal-organic framework as a new cryogenic luminescent thermometer, *J. Mater. Chem. C*, 2017, **5**, 10933–10937.
17 E. Djanffar, H. A. Bicalho, Z. Ajoyan, A. J. Howarth and H. Serier-Brault, Rare-earth UiO-66 for temperature sensing near room temperature, *J. Mater. Chem. C*, 2024, **12**, 8024–8029.
18 M. Szymczak, A. Mauri, S. Galli, L. Marciniak and M. Fandzloch, Highly sensitive, multiparametric thermal history phosphor based on an Eu(BTC) architecture, *Adv. Funct. Mater.*, 2024, **34**, 2313045.
19 T. Xia, Z. Shao, X. Yan, M. Liu, L. Yu, Y. Wan, D. Chang, J. Zhang and D. Zhao, Tailoring the triplet level of isomorphic Eu/Tb mixed MOFs for sensitive temperature sensing, *Chem. Commun.*, 2021, **57**, 3143–3146.
20 G. E. Gomez, R. Marin, A. N. Carneiro Neto, A. M. P. Botas, J. Ovens, A. A. Kitos, M. C. Bernini, L. D. Carlos, G. J. A. A. Soler-Illia and M. Murugesu, Tunable energy-transfer process in heterometallic MOF materials based on 2,6-naphthalenedicarboxylate: solid-state lighting and near-infrared luminescence thermometry, *Chem. Mater.*, 2020, **32**, 7458–7468.
21 D. Zhao, J. Zhang, D. Yue, X. Lian, Y. Cui, Y. Yang and G. Qian, A highly sensitive near-infrared luminescent metal-organic framework thermometer in the physiological range, *Chem. Commun.*, 2016, **52**, 8259–8262.
22 M. Suta and A. Meijerink, A theoretical framework for ratiometric single ion luminescent thermometers-thermodynamic and kinetic guidelines for optimized performance, *Adv. Theory Simul.*, 2020, **3**, 2000176.
23 H. Liang, K. T. Vu, P. Krishnan, T. C. Trang, D. Shin, S. Kimel and M. W. Berns, Wavelength dependence of cell cloning efficiency after optical trapping, *Biophys. J.*, 1996, **70**, 1529–1533.
24 B. del Rosal, A. Pérez-Delgado, E. Carrasco, D. J. Jovanović, M. D. Dramićanin, G. Dražić, Á. J. de la Fuente, F. Sanz-Rodriguez and D. Jaque, Neodymium-based stoichiometric ultrasmall nanoparticles for multifunctional deep-tissue photothermal therapy, *Adv. Opt. Mater.*, 2016, **4**, 782–789.
25 Y. Jin, F. Luo, Y. Che and J. M. Zheng, Decorated rutile net built on the six-connected Ln2 SBUs (secondary building units) and three-connected organic spacers, *Inorg. Chem. Commun.*, 2008, **11**, 711–713.
26 X. J. Zheng, T. T. Zheng and L. P. Jin, Self-assembly of lanthanide mixed-carboxylates coordination polymers, *J. Mol. Struct.*, 2005, **740**, 31–35.

27 M. Runowski, P. Woźny, N. Stopikowska, I. R. Martín, V. Lavín and S. Lis, Luminescent nanothermometer operating at very high temperature-sensing up to 1000 K with upconverting nanoparticles (Yb^{3+}/Tm^{3+}), *ACS Appl. Mater. Interfaces*, 2020, **12**, 43933–43941.

28 T. P. van Swieten, D. Yu, T. Yu, S. J. W. Vonk, M. Suta, Q. Zhang, A. Meijerink and F. T. Rabouw, A Ho^{3+}-based luminescent thermometer for sensitive sensing over a wide temperature range, *Adv. Opt. Mater.*, 2021, **9**, 2001518.

29 T. Amiaud and H. Serier-Brault, in *Luminescent Thermometry: Applications and Uses*, ed. J. J. Carvajal Martí and M. C. Pujol Baiges, Springer International Publishing, Cham, 2023, pp. 193–219, DOI: **10.1007/978-3-031-28516-5_5**.

30 A. M. Kaczmarek, H. S. Jena, C. Krishnaraj, H. Rijckaert, S. K. P. Veerapandian, A. Meijerink and P. Van Der Voort, Luminescent ratiometric thermometers based on a 4f-3d grafted covalent organic framework to locally measure temperature gradients during catalytic reactions, *Angew. Chem., Int. Ed.*, 2021, **60**, 3727–3736.

31 T. W. Chamberlain, R. V. Perrella, T. M. Oliveira, P. C. de Sousa Filho and R. I. Walton, A highly stable yttrium organic framework as a host for optical thermometry and D_2O detection, *Chem. – Eur. J.*, 2022, **28**, e202200410.

32 E. Hemmer, A. Benayas, F. Légaré and F. Vetrone, Exploiting the biological windows: current perspectives on fluorescent bioprobes emitting above 1000 nm, *Nanoscale Horiz.*, 2016, **1**, 168–184.

33 K. Cikalleshi, A. Nexha, T. Kister, M. Ronzan, A. Mondini, S. Mariani, T. Kraus and B. Mazzolai, A printed luminescent flier inspired by plant seeds for eco-friendly physical sensing, *Sci. Adv.*, 2023, **9**, eadi8492.

34 H. S. Jena, H. Rijckaert, C. Krishnaraj, I. Van Driessche, P. Van Der Voort and A. M. Kaczmarek, Hybrid nanocomposites formed by lanthanide nanoparticles in Zr-MOF for local temperature measurements during catalytic reactions, *Chem. Mater.*, 2021, **33**, 8007–8017.

35 C. Mi, J. Zhou, F. Wang, G. Lin and D. Jin, Ultrasensitive ratiometric nanothermometer with large dynamic range and photostability, *Chem. Mater.*, 2019, **31**, 9480–9487.

36 E. D. Martínez, C. D. S. Brites, L. D. Carlos, A. F. García-Flores, R. R. Urbano and C. Rettori, Electrochromic switch devices mixing small- and large-sized upconverting nanocrystals, *Adv. Funct. Mater.*, 2019, **29**, 1807758.

37 F. Doberenz, K. Zeng, C. Willems, K. Zhang and T. Groth, Thermoresponsive polymers and their biomedical application in tissue engineering - a review, *J. Mater. Chem. B*, 2020, **8**, 607–628.

38 Y. Yan, A. J. Faber and H. de Waal, Luminescence quenching by OH groups in highly Er-doped phosphate glasses, *J. Non-Cryst. Solids*, 1995, **181**, 283–290.

39 A. Bejan, *Heat transfer: Evolution, design and performance*, John Wiley & Sons, 2022.

40 C. Qi, S. Hou, J. Lu, W. Xue and K. Sun, Thermal characteristics of birch and its cellulose and hemicelluloses isolated by alkaline solution, *Holzforschung*, 2020, **74**, 1099–1112.

41 M. Berchel, T. L. Gall, C. Denis, S. L. Hir, F. Quentel, C. Elléouet, T. Montier, J. M. Rueff, J. Y. Salaün, J. P. Haelters, G. B. Hix, P. Lehn and P. A. Jaffrès, A silver-based metal-organic framework material as a 'reservoir' of bactericidal metal ions, *New J. Chem.*, 2011, **35**, 1000–1003.